Dipicrylamine modulates GABAρ1 receptors through interactions with residues in the TM4 and Cys-loop domains

Agenor Limon, Argel Estrada-Mondragón, Jorge M. Reyes Ruiz, Ricardo Miledi.

Neurobiology and Behavior, University of California, Irvine, 2205 McGaugh Hall, Irvine California 92697, United States. AL, JMRR, RM

Psychiatry and Human Behavior, University of California, Irvine, 2226 Gillespie NRF, Irvine California, 92697, Unites States. AL

The Queensland Brain Institute, QBI Building (number 79), St. Lucia, Queensland 4072, Australia. AEM

1

Running Title:

DPA effects on LGIC receptors

Corresponding author:

Agenor Limon,
2226 Gillespie NRF
Irvine CA; 92697-1675
alimonru@uci.edu

Number of text pages: 31

Tables: 1 in main text and 1 in Supplemental material

Figures: 8 in main text and 5 in Supplemental material

References: 42

Words in abstract: 250

Introduction: 380

Discussion: 1522

List of abbreviations:

$GABA_A Rs$, $GABA_A$ receptors

DPA, dipicrylamine

LGIC, ligand gated ion channels;

BSA, bovine serum albumin

Abstract

Dipicrylamine (DPA) is a commonly used acceptor agent in Förster resonance energy transfer (FRET) experiments that allows the study of high frequency neuronal activity in the optical-monitoring of voltage in living cells. However, DPA potently antagonizes $GABA_A$ receptors ($GABA_A$Rs) that contain $\alpha1$ and $\beta2$ subunits by a mechanism which is not clearly understood. In this work, we aimed to determine whether DPA modulation is a general phenomenon of Cys-loop ligand-gated ion channels (LGICs) and whether this modulation depends on particular amino acid residues. For this we studied the effects of DPA on human homomeric GABAρ1, $\alpha7$ nicotinic and $5\text{-}HT_{3A}$ receptors expressed in *Xenopus* oocytes. Our results indicate that DPA is an allosteric modulator of GABAρ1 receptors with an IC_{50} of 1.6 µM, an enhancer of $\alpha7$ nicotinic receptors at relatively high concentrations of DPA, and has little, if any, effect on $5\text{-}HT_{3A}$ receptors. DPA antagonism of GABAρ1 was strongly enhanced by pre-incubation, was slightly voltage-dependent, and its washout was accelerated by bovine serum albumin. These results indicate that DPA modulation is not a general phenomenon of LGICs and structural differences between receptors may account for disparities in DPA effects. In silico modeling of DPA docking to GABAρ1, $\alpha7$ nicotinic, and $5\text{-}HT_{3A}$ receptors suggests that a hydrophobic pocket within the Cys-loop and the M4 segment in GABAρ1, located at the extracellular/membrane interface, facilitates the interaction with DPA that leads to inhibition of the receptor. Functional examinations of mutant receptors support the involvement of the M4 segment in the allosteric modulation of GABAρ1 by DPA.

Introduction

Dipicrylamine (DPA) is a hydrophobic anion that intercalates into cellular membranes (Wang and Bruner, 1978) and has been broadly used as a probe to study the physical and biological properties of cellular membranes (Chanda et al., 2005; Kleijn et al., 1983; Oberhauser and Fernandez, 1995). Notably, DPA allows the study of high frequency neuronal activity in the optical-monitoring of voltage in living cells (Bradley et al., 2009); however, the compound's unexpected effects on GABA$_A$ receptors (GABA$_A$Rs) and NMDA receptors have imposed limits on its broad physiological applications (Chisari et al., 2011; Linsenbardt et al., 2012). Thus, a better understanding of the mechanisms involved in DPA's effects would be helpful for effective modifications of the DPA molecule to reduce or eliminate its pharmacological activity while preserving its key optical characteristics. Thus far, the mechanism and specificity of the DPA inhibition of GABA$_A$Rs remains elusive (Chisari et al., 2011). Two non-mutually exclusive scenarios may explain DPA's effects. In one scenario, DPA may trigger unspecific local perturbations in the surrounding protein/lipid interphase that are responsible for conformational changes in the receptor and altered gating. In the other scenario, the antagonism is mediated by site-specific interactions between DPA and transmembrane sites of the receptor (Chisari et al., 2011; Mennerick et al., 2008).

To explore the potential mechanism for DPA's effects, we investigated whether DPA also affects human GABA receptors that are composed of ρ1 subunits (GABAρ1 receptors). The homomeric nature of this receptor is advantageous for structural modeling studies compared with heteromeric GABA$_A$Rs composed of GABA α, β, and γ subunits. After demonstrating that DPA also negatively modulates GABAρ1 receptors, we compared in silico structural models and the DPA inhibition of homomeric GABAρ1, α7 nicotinic receptors (nAChRα7), and 5-HT$_{3A}$

receptors to identify structural motifs with the potential to interact with DPA. Finally, we performed a mutagenesis analysis of the GABAρ1 subunit to determine the congruence between the structural model and DPA effects. Our results demonstrate that DPA is an allosteric modulator of GABA$_A$Rs and exhibits pharmacological effects on α7 nicotinic ACh receptors but little, if any, effects on 5-HT$_{3A}$ receptors. The aromatic residue W475, which is located in the upper part of the transmembrane domain 4 (TM4) of GABAρ1, appears to participate in the gating of the receptor and in the DPA-mediated inhibition of GABAρ1 receptors.

Materials and Methods

Molecular biology

For the experiments using GABA$_A$Rs, we used mRNA that was isolated from rat brain cortices using the FastTrack 2.0 kit (Invitrogen, Carlsbad, CA). For the expression of homomeric channels, we used human α7 nicotinic receptor cDNA (donated by Professor Eleonora Palma; Universita di Roma La Sapienza), human 5-HT$_{3A}$ cDNA (purchased from Missouri S&T cDNA Resource Center), and GABAρ1, which was cloned from a human retina cDNA library (Martinez-Torres et al., 1998), and introduced the genes into pcDNA3 (Invitrogen, Carlsbad, CA). These plasmids were transformed into the *Escherichia coli* DH5α strain for storage and amplification. Linearized plasmids were used as templates for cRNA synthesis using the Ambion's mMessage mMachine kit (Ambion, Austin, TX). Stage V–VI *Xenopus* oocytes were injected with 50 nl of mRNA or cRNA (concentration of 1 mg/mL) and then maintained in Barth's solution [88 mM NaCl, 0.33 mM Ca(NO$_3$)$_2$, 0.41 mM CaCl$_2$, 1 mM KCl, 0.82 mM MgSO$_4$, 2.4 mM NaHCO$_3$, 10 mM HEPES (pH 7.4)] with 100 U/mL of penicillin and 0.1 mg/mL of streptomycin (Sigma; St Louis, MO) at 16-17 °C until the moment of recording.

Electrophysiological assay

The oocytes were harvested and prepared as previously described (Miledi et al., 2006), with slight modifications as noted below. Briefly, *Xenopus laevis* frogs were anesthetized in tricaine methane sulfonate (MS-222, 0.17%) and euthanized by decapitation, in adherence to protocols approved by the University of California Institutional Animal Care and Use Committee. The ovarian lobes were removed, cut into small pieces and placed in Ca^{2+}-free Barth's solution with 2 mg/ml collagenase type I (Sigma) for 2 hr in constant rotation. After the enzymatic treatment, isolated stage V–VI oocytes were selected and maintained at 17 °C for the remainder of the experiment. Healthy looking oocytes were injected approximately 24 hr after enzymatic dissociation. Three to four days after injection, the oocytes were impaled with two microelectrodes filled with 3 M KCl and voltage clamped at -80 mV using a two-electrode voltage clamp amplifier (Miledi, 1982). The oocytes were continuously perfused with gravity-driven frog Ringer's solution [115 mM NaCl, 2 mM KCl, 1.8 mM $CaCl_2$, 5 mM HEPES (pH 7.4)] at room temperature (19–21 °C). Data acquisition was performed using WinWCP V 3.9.4 (John Dempster, Glasgow, United Kingdom), as previously reported (Limon et al., 2010; Ochoa-de la Paz et al., 2012). DPA was purchased from Biotium (Hayward, CA). The rest of the substances used were obtained from Sigma-Aldrich (St. Louis, MO).

Data analysis

The antagonist effect of DPA on GABA currents was determined by measuring the percent inhibition produced by different concentrations of DPA. The concentration of DPA causing a 50% decrease in GABA currents (IC_{50}) was estimated by fitting the following logistic equation to the experimental data: $I = I_{min} + (I_{max} − I_{min})/[1 +(x/IC_{50})k]$ (Origin 8.5), in which x is

the concentration of DPA (in M), I is the amplitude of the agonist response (in nA), and k is the

slope of the curve. The EC_{50} and the Hill coefficient were determined by fitting the Hill equation

in the form $I = I_{max}/(1+(EC_{50}/[A])^{n})$, in which I is the current amplitude, I_{max} is the maximum

current amplitude at the concentration of the agonist [A], EC_{50} is the agonist concentration that

induces 50% of the maximal response, and n is the Hill coefficient. The time constants of

activation and deactivation were measured by fitting a simple exponential equation between the

10-90% of the rise and decay current using Clampfit v.10.0 software (Molecular Devices). The

experimental data are shown as the mean $\pm$ S.E.M. Statistical differences were determined by

Student's t-test when comparing a pair of responses and by Dunnett's test when making multiple

comparisons with respect to the GABAρ1 wild type receptor (WT) (JMP v. 10; SAS Institute).

We considered two groups significantly different when $P < 0.05$.

Homology modeling

Three homology models of the GABAρ1, α7 nicotinic and 5-HT$_{3A}$ subunits were built.

The first model was based on the recently published structure of the β3 homomeric human

GABA$_A$ receptor (PDB code 4COF, (Miller and Aricescu, 2014)), and the last two models used

the structure of the nicotinic acetylcholine receptor from the *Torpedo marmorata* electric organ

(PDB code 4AQ9, (Unwin and Fujiyoshi, 2012)). We employed MODELLER v9.12 (Sali and

Blundell, 1993) and built 20 models of each subunit by applying the respective alignments of the

UniProt code sequences: P24046 (GABA ρ1), P36544 (α7 nicotinic), and P46098 (5-HT3$_A$)

(Supplementary Figures 1 and 2). Then, in each case, we chose the best model based on the TM

score and RMSD.

Each subunit was then projected five-fold onto their respective template using Molsoft

ICM-Pro v3.5 (Totrov and Abagyan, 1997), and the few clashes observed at the interfaces were

7

removed by local energy minimization. The entire pentamers were refined by energy

minimization using the internal coordinate space, followed by optimizing the geometry of the

built structures with a fast Dreiding-like forcefield employing Accelrys Discovery Studio v2.5

(Chen et al., 2006). The human GABAρ1 subunit is 52%, 56% and 61% homologous to the

GABA subunits α1 (Uniprot P14867), γ2L (Uniprot P18507) and β3 (Uniprot P28472),

respectively. Because the structure of the homomeric β3 GABA receptor was recently solved

(Miller and Aricescu, 2014) and GABA ρ1 and β3 form homomeric receptors and have high

homology we think that using β3 as a template can give us a better estimation about the

physiological and molecular aspects of the receptor interacting with dipicrylamine.

Molecular docking

We used Pocket Finder in ICM, as previously reported (Dey and Chen, 2011). Briefly,

three (GABAρ1), four (α7 nicotinic), or eight (5-HT3$_A$) sites per subunit were identified by the

automatic detection of small molecule binding sites on the homomeric receptors (Supplemental

Figure 3); then, one copy of the 3D structure of DPA (2,4,6-trinitro-N-(2,4,6-

trinitrophenyl)aniline) was loaded from ChemSpider into the ICM project (CSID:8258,

http://www.chemspider.com/Chemical-Structure.8258.html). The estimated octanol/water

partition coefficient of DPA (log Kow = 3.35) indicates that the compound would be poorly

soluble in water; thus, we only considered sites that were located at the extracellular/membrane

interface (II in GABAρ1; I in α7 nicotinic; and II and III in 5-HT3$_A$) as putative sites for

allosteric modulation. One or two molecules were accommodated in each pocket by applying a

second local energy minimization. The same procedure was done to dock DPA molecule to the

heteromeric model of GABA$_A$ receptor. The images were made using ICM and PyMOL v

1.5.0.4.

Results

DPA's effects on GABA$_A$Rs

To determine whether the DPA antagonism originally described for the $\alpha1\beta2$ and $\alpha1\beta2\gamma2$

GABA$_A$Rs extends to other endogenous GABA$_A$Rs we evaluated DPA effects on oocytes that

were previously injected with mRNA isolated from rat brain cortex. These mRNA-injected

oocytes express a large variety of GABA$_A$Rs that are representative of those expressed in the rat

brain (Demuro et al., 1999). To ensure maximum activation of all subtypes of mRNA-expressed

GABA$_A$Rs we tested DPA with saturating concentrations of GABA. In agreement with Chisari

et al., the coapplication of GABA and DPA reduced the peak and accelerated the decay of

GABA currents in a concentration-dependent manner (Fig. 1A, C). This result indicates that the

DPA antagonism described for $\alpha1\beta2$ and $\alpha1\beta2\gamma2$ GABA$_A$Rs is qualitatively similar in

GABA$_A$Rs that were expressed by endogenous rat brain mRNA. Notably, the recovery from

DPA inhibition was not complete even after 30 min; therefore, to avoid cumulative effects on the

concentration response experiments, each oocyte was tested with DPA only once. The IC$_{50}$ of the

aqueous DPA concentration was 62 ± 11 nM (n = 3–5 oocytes per concentration), which is a

value similar to that reported for the DPA inhibition of GABA$_A$Rs with $\alpha1\beta2\gamma2$ stoichiometry

(65 nM) (Chisari et al., 2011).

DPA antagonism of homomeric GABAρ1 receptors

GABAρ1 receptors exhibit a high affinity for GABA, demonstrate slow desensitization and have

a pharmacological profile so distinctive that for approximately two decades they were classified

as $GABA_C$ (Martinez-Delgado et al., 2010). Therefore, we investigated whether GABAρ1 receptors were modulated by DPA. Figure 1B-C shows that the coapplication of DPA and GABA inhibited the maximal response of GABAρ1 receptors with an IC_{50} of 1.57 ± 0.2 μM (n = 4). The effects of DPA on GABAρ1 kinetics were different than those observed on $GABA_ARs$ from rat brain cortices (Fig. 1A) and heterologously expressed α1β2γ2 receptors (Chisari et al., 2011). The GABAρ1 receptors exhibited a tail current at the end of the GABA and DPA coapplication (Fig. 1B), indicating that inhibition by DPA is partially relieved faster than the deactivation of GABAρ1 channels is completed.

DPA also produced a 5-fold dextral displacement of the concentration/response curve for GABA (Fig. 2), increasing the EC_{50} from 0.91 ± 0.3 μM to 4.59 ± 1.6 μM (n = 3–5 oocytes per point; p = 0.031; Fig. 2A, B), and a reduction of the Hill coefficient from 2.34 ± 0.3 to 1.07 ± 0.25 (p = 0.001). DPA antagonism was not surmounted by increasing the concentration of GABA, a result that is consistent with the non-competitive, negative allosteric modulation of the GABAρ1 receptor (Fig. 2B). Notably, the antagonism of the GABAρ1 receptor was enhanced by preincubation with DPA. Without preincubation, the coapplication of 5 μM DPA and GABA reduced the maximum current by $15 \pm 3\%$ (n = 5; Fig. 2B, black triangle); however, when DPA was preincubated for 3 min, the GABA efficacy was reduced by $91.1 \pm 1.7\%$ (n = 5; white triangles in Fig. 2B), indicating that the DPA antagonism of $GABA_AR$ has a slow onset rate. Given the effects of DPA preincubation on GABA efficacy we also studied the effect of 3 μM DPA, preincubated by 200 s, on the concentration/response dependence of GABAρ1 receptors (Fig. 2B). In this condition 3 μM DPA reduced the maximal GABA efficacy by $77 \pm 6.6\%$ and doubled the EC_{50} for GABA from 0.91 in control to 2.0 ± 0.16 μM (n = 4 oocytes; p = 0.021), without affecting the Hill coefficient (2.34 to 1.9 ± 0.14; n = 4 oocytes, p = 0.263).

10

Further experiments demonstrated that the percentage of DPA inhibition exponentially

increased, with the incubation time reaching a maximum after approximately 3 min (Fig. 3A, B).

The percentage of maximal inhibition was greater when the oocytes were tested with DPA only

once (91.1 ± 1.7%; Fig. 3A, B) than when they were tested consecutive times (maximum

inhibition of 42.4 ± 7.6%; n = 4; data not shown), suggesting incomplete recovery from DPA's

effects between applications, even after washout periods of more than 20 min. Chisari et al.,

previously reported that bovine serum albumin (BSA) a molecular scavenger of DPA accelerated

DPA membrane removal and the antagonism offset of GABA$_A$Rs (Chisari et al., 2011);

therefore, we analyzed whether a similar mechanism was present in DPA antagonism of

GABAρ1. In our experiments BSA also accelerated DPA washout (Fig. 3C, D) reducing the τ of

antagonism offset from 36.2 ± 5.3 s in absence of BSA to 16.8 ± 1.7 s in presence of BSA (p =

0.014; n = 4). This result indicates that incomplete recovery of DPA can be explained by

incomplete DPA membrane removal.

Voltage dependence of DPA inhibition

Partitioned DPA is negatively charged and generates charge movements when translocating

within the plasma membrane in response to changes in voltage. Previous studies have indicated

that DPA's charge movements in oocyte membranes can be described by a Boltzmann function

with V$_{1/2}$ for oocytes of -54 and -59 mV for injected and uninjected oocytes, respectively

(Chisari et al., 2011), we performed similar experiments in non-injected oocytes and obtained a

V$_{1/2}$ of -55 ± 2.3 mV (n = 6) (Figure 4A). Therefore, we investigated whether the effects of DPA

on GABAρ1 also varied with changes in voltage. For this study, we exploited the slow

desensitization of GABAρ1-mediated currents that facilitate the use of voltage ramp protocols to

measure the effects of DPA on steady-state currents. A steady-state GABA current was obtained

11

by subtracting the current elicited by a voltage ramp protocol from -90 mV to +65 mV (80 mV/s)

under control conditions from the ramp-elicited current after the response to 1 µM GABA

reached an equilibrium (Figure 4). The sensitivity of any oocyte's endogenous component to 3

µM DPA was determined by subtracting the ramp-elicited currents before and after 200 s of

incubation with DPA. The fraction of steady-state GABA current available after 200 s of 3 µM

DPA preincubation was obtained by subtracting ramp-elicited currents with DPA from those

elicited during the coapplication of 3 µM DPA and 1 µM GABA.

The inversion potential of GABA currents (E_{GABA}) before and after DPA was -25.4 ± 3.1 mV

and -21.8 ± 1.6 mV, respectively, indicating that DPA did not affect the permeability of the

channel (n = 5, p = 0.33). We did observe a small but significant voltage dependence for DPA

modulation of the GABAρ1 receptor. Figure 4C shows that the percentage of inhibition of the

GABA current linearly decreased with positive voltages between 0 and +60 mV (r^2 = 0.99);

however, at negative voltages down to -60 mV, the percentage of inhibition remained

unchanged, regardless of the voltage. We did not extend the voltage ramp protocol beyond +65

mV because more positive voltages are not normally observed in physiological conditions.

Moreover, because the percentage of inhibition trends asymptotically to ± ∞ when close to

E_{GABA}, we excluded from the analysis the voltage range in which the percentage of inhibition

could not be reliably calculated. For comparison purposes, we calculated the DPA-mediated

inhibition of the steady-state GABA current at -90 and +50 mV. As observed in Figure 4, DPA

reduced the steady-state GABA current to 20.1 ± 5.3% and 35 ± 5.1% of the control at -90 and +

50 mV, respectively (n = 5, p < 0.001, paired Student's *t*-test). Additionally, we also measured

the onset rate of DPA antagonism at -90 and +50 mV once the current was already activated.

Figure 4E-G shows that DPA inhibition of the GABA current was faster at -90 mV than at +50

mV. The best fit for the onset of DPA's effects was the sum of two exponential functions with the time constants τ_1 2.0 ± 0.9 s and τ_2 9.6 ± 1.6 s at -90 mV (n = 5) and τ_1 2.3 ± 0.1 s and τ_2 16.9 ± 1.8 s at +50 mV (n = 5). τ_2 was significantly slower at positive voltages (p < 0.05, Student's *t*-test) (Fig. 4F).

Previous studies, and our own results, indicate that DPA's charge movements in oocyte membranes can be described by a Boltzmann function with $V_{1/2}$ of approximately -54 mV; therefore, at membrane potentials of -90 mV, the concentration of DPA is expected to be higher in the outer leaflet of the plasma membrane. The faster onset of DPA antagonism at negative potentials suggests that inhibition is favored when DPA molecules are near the protein-lipid interface at the upper part of the receptor. In addition, depolarization during ramp protocols should translocate free or weakly bound DPA with a $V_{1/2}$ of approximately -55 mV; however, our experiments indicate that a partial removal of steady-state antagonism is observed at values more positive than 0 mV. This result suggests that depolarizing voltages are not sufficient to counter a) the affinity of DPA for the activated receptor and/or b) the slow kinetics of DPA dissociation (see below in discussion).

DPA effects on homomeric receptors of the LGIC family

The GABA ρ1 and α1 subunits are only 33% homologous, and receptors containing either of these subunits exhibit profound pharmacological differences. Nevertheless, ρ1 and α1β2 GABA receptors are both antagonized by DPA. Based on the effects of DPA on GABAρ1, we hypothesized that if DPA also modulated other homomeric members of the Cys-loop LGIC family, then we could perform comparative studies between the functional effects of DPA and

13

the structure of those receptors. Therefore, we evaluated the effects of DPA on homomeric 5-HT$_{3A}$ and α7 nicotinic receptors.

DPA did not significantly modify the maximal response of 5-HT$_{3A}$ receptors elicited by a high concentration of 5-HT (10 μM) (Fig. 5); small changes in the desensitization of 5-HT-elicited currents were not significant upon statistical testing ($P > 0.05$, paired Student's t-test). By contrast, α7 nicotinic receptors were modulated by high concentrations of DPA. Whereas 1 μM DPA exhibited almost no effect on maximal α7 nicotinic receptor responses elicited by a saturating concentration of ACh (100 μM) (97 ± 8% of control; n = 5), 5 μM DPA increased the peak of ACh-elicited currents by 91 ± 15% (n = 12; Fig. 5). The potentiation of α7 nicotinic receptors by DPA was observed only for the current activation, with no effect on the desensitization.

In silico modeling of a binding domain for DPA in homomeric receptors of the LGIC family

The differential effects of DPA on GABAρ1, α7 nicotinic and 5-HT$_{3A}$ homopentameric receptors provided an opportunity to further examine the structural components of the receptors that might interact with DPA. We created an in silico model of each receptor. Each model displayed a different pattern of potential pockets that can interact with DPA throughout their extracellular and transmembrane domains, according to their particular architecture. Because the partition coefficient of DPA predicts poor solubility in water, we only considered sites that were located at the extracellular/membrane interface as putative sites for allosteric modulation in each case. The 5-HT$_{3A}$ receptor contains two sites that are each able to accommodate one molecule of DPA, whereas the GABAρ1 and α7 nicotinic receptors display enough space to contain just one molecule at the protein-lipid interface in each subunit (sites II in GABAρ1, I in α7 nicotinic, and

II and III in 5-HT3$_A$; Supplemental Figure 3). These sites were located in the upper half of the

transmembrane domain near the superior limit of the membrane in all of the models (Figure 6).

We identified several hydrophobic aromatic residues interacting with DPA in the three

models and/or positively charged arginine residues in the GABAρ1 and α7 nicotinic receptors.

These residues include L207, I281, L285, Y289, Y474, and W475 in GABAρ1; F157, F159,

R227, Y296, F297, and F493 in α7 nicotinic receptors; and F166, F164, F309, and W472 in the

5-HT$_{3A}$ receptors (Figure 6). The pattern appears to indicate the existence of certain acidic

recognition motifs rich in aromatic, hydrophobic and even positively charged amino acids that

provide π-stacking and electrostatic contributions to stabilize the structure of DPA. This

conserved pocket formed by amino acids in the Cys-loop, M1 and M4 domains is reminiscent of

the general anesthetic cavity that was reported by Nury et al. (Nury et al., 2011), notwithstanding

that the specific residues that interact in each case induce a very different physiological response.

Previous results demonstrated that a point mutation in the transmembrane domain 2 of the α1

subunit (V256S) that renders α1β2 and α1β2γ2 receptors insensitive to pregnenolone sulfate

(PS)(Akk et al., 2001) also removes sensitivity to DPA(Chisari et al., 2011). Akk et al.,

originally described the mutation and concluded that this residue is unlikely to be part of the

binding site for PS and may influence PS action indirectly. In agreement with that interpretation,

our model of GABAρ1 does not predict interactions between the DPA and the residue equivalent

to V256 in α1β2.

Interactions between DPA and in silico heteromeric α1β2γ2 GABA$_A$ receptor

To explore possible interactions between V256 and DPA in heteromeric GABA receptors we

used a model of α1β2γ2 (Estrada-Mondragon and Lynch, 2015)(Supplemental Figure 4), in this

15

model V256 in $\alpha1\beta2\gamma2$ does not interact with DPA indicating that V256 is most likely involved in the signal transduction mechanisms following binding by DPA to another site. We also explored hydrophobic pockets in the $\alpha1\beta2\gamma2$ model; interestingly, $\alpha1$ and $\rho1$ subunits share the same pattern of interactions with DPA, with basically the same equivalent residues able to accommodate one DPA molecule in the hydrophobic pocket (Supplemental Figure 4). In the other hand, $\gamma2$ and $\beta2$ are able to accommodate two DPA molecules each; however, the interactions resemble more those described for the 5-HT$_{3A}$ receptor, where the impact in the function is minimal. Our model predicts that interactions of DPA with the $\alpha1$ subunit are strong drivers of non-competitive antagonism of DPA in heteromeric GABA$_A$ receptors. These interactions do not discard that additional non-specific membrane perturbations also participate in the inhibition of these receptors. Future comparative studies between heteromeric and homomeric GABA$_A$ receptor should provide more information regarding the differences in DPA antagonism between these receptors.

DPA effects on GABA$\rho1$ receptors with structural modifications on M4

Because amino acids at the end of the M4 domain appear to be important for DPA binding and because interactions between M4 and the Cys-loop are necessary for channel activation (Estrada-Mondragon et al., 2010), we studied the effects of the DPA-mediated antagonism of GABA$\rho1$ receptors mutated in the M4 domain.

We tested the effects of DPA on GABA$\rho1$ mutants in which the C-termini of the M4 was shortened by 1 (S479X or GABA$\rho1$-1aa), 2 (F478X or GABA$\rho1$-2aa), or 3 (I477X or GABA$\rho1$-3aa) amino acids (Reyes-Ruiz et al., 2010). These mutants exhibited clear changes in their

16

kinetic properties when activated with GABA (Reyes-Ruiz et al., 2010). Whereas the deletion of

1 amino acid slowed the activation and decay of the current, the deletion of 2 amino acids greatly

accelerated both parameters (Table 1), suggesting a close involvement of the M4 end termini in

the gating of the GABAρ1 receptor. To test the effects of DPA, we preincubated the receptors

with 1 μM DPA for 180 s and then co-treated them with DPA and the EC_{50} concentration of

GABA for each receptor subtype (see Table 1); this procedure allows for the maximal

antagonism of DPA at the EC_{50} while reducing acute nonspecific effects of DPA on the

membrane. Using this procedure, we found that the deletion of up to 2 amino acids did not affect

DPA-mediated antagonism (Fig. 7). However, DPA antagonism was modestly enhanced in the -

3aa mutant, blocking GABA currents by $76.4 \pm 1.3\%$ in GABAρ1-3aa vs. $68.7 \pm 0.9\%$ in WT (n

$= 6$; $p = 0.002$; Fig. 7).

The amplitude of the post-DPA current tail was positively correlated with the decay time of the

GABA currents ($r = 0.93$; Supplemental Figure 5). The largest tail was observed in GABAρ1-

1aa and was absent in GABAρ1-2aa; these were the mutants with the highest and lowest

deactivation time constants, respectively (Fig. 7 and Table 1). This result indicates that the post-

DPA tail arises from speed differences in GABA current decay and relief from DPA antagonism.

Further shortening of M4 produced nonfunctional receptors (Reyes-Ruiz et al., 2010).

Next, we examined the role of the residue W475 that our model implicated in the charge

stabilization of DPA within the hydrophobic pocket of each GABAρ1 subunit. As previously

demonstrated, the substitution of W475 by electrically charged amino acids (W475R and

W475D) produced nonfunctional receptors, indicating the fundamental role of W475 in the

gating of the receptor (Estrada-Mondragon et al., 2010). The substitution of W475 with

17

hydrophobic amino acids (W475F, W475L, W475G, and W475A) produced functional channels with less sensitivity and lower efficacy in response to GABA and faster kinetics, and all of the mutants except W475L demonstrated less cooperativity (as reported by the Hill coefficient) than the WT receptor (Table 1). Despite the differences in kinetic and affinity properties between mutants and the WT receptor, we did not observe a statistically significant difference in the antagonistic activity of DPA against W475F, W475L, and W475G with respect to the WT receptor; however, W475A was less sensitive to DPA than the WT receptor (Fig. 7). The IC_{50} for DPA antagonism, measured after 3 min preincubation with DPA, of W475A's EC_{50} was significantly higher (843 ± 35 nM; n = 4, p< 0.001, Dunnett's method) than that for W475F (383 ± 38 nM; n = 4) and WT (309 ± 30 nM; n = 4).

Discussion

In this study we report for first time that DPA is a negative allosteric modulator of GABAρ1 and a potentiator of $\alpha 7$ nicotinic receptors, with no detectable effects on 5-HT_{3A} receptors. The differential pharmacological effects of DPA on distinct receptors of the Cys-loop LGIC family are supportive of a mechanistic model in which DPA modulates receptor activity via site-specific interactions located within transmembrane segments.

Interactions between DPA and in silico homomeric LGIC channels

By using the recently published structure of the anionic β3 homomeric human GABA$_A$R (Miller and Aricescu, 2014), we adjusted the previous GABAρ1 model (Estrada-Mondragon et al., 2010), which now exhibits a higher alignment score in homology and identity (Supplemental Figures 1 and 2). Our new GABAρ1 model predicts interactions between the DPA molecule and

18

several residues located in the upper half of the transmembrane domain to form a hydrophobic

cavity that encages DPA in a very stable conformation. This hydrophobic cavity is located

behind the upper part of the pore. Recent progress in the search of the gating mechanism along

the channel indicates that the upper half of the pore that is lined by the M2 domain of each

subunit undergoes considerable deformation, being functionally coupled through loop M2-M3

with loop 2 of the extracellular domain during ligand-induced activation (Prevost et al., 2012;

Unwin and Fujiyoshi, 2012). Lipids contribute in a fundamental way to achieve this coupling

through critical points conferred by few hydrophobic residues and by electrically charged

residues in such interphases (daCosta et al., 2009; Estrada-Mondragon et al., 2010; Fernandez

Nievas et al., 2008). Our previous studies have demonstrated that at least two amino acids that

form the hydrophobic cavity for DPA, W475 in TM4, and L207 in the Cys-loop participate in

planar hydrophobic interactions that are necessary for the activation of the GABAρ1 channel

(Estrada-Mondragon et al., 2010); therefore, the presence of DPA inside the hydrophobic pocket

may hinder physiological TM4-Cys-loop interactions, which in turn alter the gating of the

channel (see below).

A similar cavity was identified in α7 nicotinic receptors, wherein an entire hydrophobic

aromatic network distributed along the neighboring pre-TM1 and Cys-loop domains appears to

interact with DPA. Based on the potentiation effects elicited by DPA, DPA interactions in this

cavity may promote energetic coupling stacking by narrowing the distance between the aromatic

residues in the TM1 and Cys-loop domains and those in the TM2-TM3 domain because the

participation of inter-residue coupling in these domains is known to be important for rapid and

efficient gating of the nicotinic receptor, as described by (Lee et al., 2009).

19

In the case of the cationic 5-HT$_{3A}$ receptor, the interface between extracellular and transmembrane domains appears to be quite different from those of anionic LGIC receptors and even significantly different from cationic receptors such as α7 nicotinic receptors (Bouzat et al., 2008). Certain charged residues that have been identified as key elements for channel activation, such as R241 in the pre-TM1 domain (Hu and Peoples, 2008; Hu et al., 2003) and K76 in loop 2 (Reeves et al., 2005), are located a considerable distance away from the docked position of DPA molecules in our model. In fact, these regions are only stabilized loosely by hydrophobic residues close to the membrane upper leaflet and are substantially distant from any charged residue. The lack of DPA effects on the 5-HT$_{3A}$ receptor indicates that the presence of the hydrophobic pocket where DPA fits is not enough requirement for antagonism; in addition, appropriate stabilization of DPA's charge and interaction with amino acids involved in gating of the channel is necessary for allosteric modulation by DPA.

We propose that although the interface of interaction is very similar among the different receptors, the specificities of each receptor induce a very different response, which fits well and complements the data presented here.

Allosteric modulation of GABAρ1 by DPA

Our GABAρ1 model suggests that bound DPA alters the gating of the channel by affecting interactions between W475 in TM4 and L207 in the Cys-loop domains. Evidence of allosteric modulation and gating alterations is further provided by the exponential slow onset of DPA antagonism of the GABA current. Our model predicts 5 binding sites for DPA in each pentameric GABAρ1 receptor, with one per subunit. Although we do not know how many DPA molecules are required to inhibit the receptor, we hypothesize that a) the open probability of

20

GABAρ1 is negatively correlated with the number of DPA molecules bound to the receptor and

b) the affinity of available binding sites for DPA is progressively reduced after each site is

occupied by additional DPA molecules. This negative cooperativity between binding sites for

DPA would also contribute to the complex recovery effects of GABAρ1. The presence of a post-

DPA current tail indicates that a fraction of DPA inhibition is relieved faster than the

deactivation of GABAρ1 channels, thus generating faster K_{off} than 0.18 s^{-1} (Chang and Weiss,

1999); however, the slow recovery of DPA effects also suggests that at least one additional

substantially slower K_{off} exists for DPA dissociation. Notably, although the mechanism of DPA-

mediated antagonism is likely distinct from that of picrotoxin antagonism, the post-DPA tail

current of GABAρ1 occurs in a highly similar fashion to the post-picrotoxin tail current

described for perch GABAρ1 (Qian et al., 2005). Future determination of the constant rates for

DPA inhibition and equilibrium modeling may help to decipher the sequential states of DPA

binding to GABAρ1; however, based on the results using BSA, realistic models should

contemplate the kinetics of DPA partitioning-departitioning in the cell membrane.

DPA antagonism reduced GABA efficacy and produced a right-shift displacement of

the concentration response curve; because affinity is influenced by the gating of the receptor

(Chang and Weiss, 1999; Colquhoun, 1998) at this stage, we cannot discard the possibility that

conformational changes affecting the affinity for GABA participate in DPA-mediated inhibition

of GABA responses. However, a single point mutation of W475 generates GABA receptors with

very distinct apparent affinities and distinct decay times. The measurement of binding and

activity in the same oocyte demonstrated that the slow decay of the GABA current in GABAρ1

results from the lock-on of bound GABA while the receptor is in the open state (Chang and

Weiss, 1999). If the same mechanism is preserved in the mutants studied here, a faster decay of

the GABA current would reflect a faster transition of GABAρ1 from the active to the closed

state. Because previous studies have already demonstrated that a reduction of the channel

opening rate may lead to larger EC_{50} values and lower efficacy (Chang et al., 2000), we

hypothesize that mutants with faster decays will display higher GABA EC_{50} values and lower

efficacy. Indeed, Figure 8 shows a linear correlation between the time constant of GABA current

decay and the EC_{50} for GABA. Moreover, the maximal response to GABA was reduced by

several fold in all W475 mutants (Table 1). Because the post-DPA tail and decay time are

correlated, we also analyzed the relationship between the post-DPA tail and the EC_{50} for GABA.

Interestingly, the amplitude of the post-DPA tail, in terms of the percentage of the maximal

current, fell exponentially with increases in the apparent GABA affinity of the receptor (Fig.

8B). The Hill coefficient was negatively correlated with EC_{50} in the mutants, which can be

interpreted as a reduction in the cooperativity produced by alterations in gating. Interestingly,

only the W475A mutant exhibited a reduction in DPA antagonism, and we did not find any

correlation between the % of antagonism and any of the kinetic or pharmacological parameters

studied here (Supplemental Table 1). Evidently, W475 is a very important residue for gating

transduction of the channel, substitution of polar residues renders non-functional receptors and

point mutations produces channels with varied characteristics. While it is not surprising that

DPA inhibition was not affected by W475F and W475L mutants, as they are very similar to

W475 in terms of hydrophobicity and steric effect, the differential effects Ala and Gly

substitution at the 475 position are puzzling. Both residues are small, hydrophobic and

compatible with the accommodation of DPA in the transmembrane domain, thus differences in

size are not a compelling reason to explain the differential effect on DPA antagonism; however,

it is known that Ala and Gly are at opposite extremes of their capacity to bury hydrophobic area

within α-helical structures (Scott et al., 2007). It may be possible that Ala reduces the general

hydrophobicity of DPA pocket, compared to Gly, reducing the stabilization of the DPA molecule

and decreasing the antagonism of the receptor.

Taken together, the results suggest to us that the DPA-mediated antagonism of

GABAρ1 results mainly from alterations in receptor gating via interactions with amino acids

forming a hydrophobic cavity in the upper part of the channel. This cavity appears to be

conserved in members of the Cys-loop LGIC family and would be equivalent to the hydrophobic

pocket near the interphase of the membrane and the extracellular domain that was identified by

photolabeling and nuclear magnetic resonance (NMR) in nAChRs (Bondarenko et al., 2013;

Chiara et al., 2009) and by electron paramagnetic resonance (EPR) spectroscopy and X-ray

crystallography in the prokaryotic GLIC (Nury et al., 2011; Velisetty and Chakrapani, 2012).

Acknowledgments.

Authorship contributions.

Participated in research design: Limon, Estrada-Mondragon, Reyes-Ruiz.

Conducted experiments: Limon, Estrada Mondragon.

Contributed new reagents or analytic tools: Reyes-Ruiz, Miledi.

Performed data analysis: Limon, Estrada Mondragon.

Wrote or contributed to the writing of the manuscript: Limon, Estrada-Mondragon, Reyes-Ruiz, Miledi.

References

Akk G, Bracamontes J and Steinbach JH (2001) Pregnenolone sulfate block of GABA(A) receptors: mechanism and involvement of a residue in the M2 region of the alpha subunit. *J Physiol* **532**(Pt 3):673-684.

Bondarenko V, Mowrey D, Liu LT, Xu Y and Tang P (2013) NMR resolved multiple anesthetic binding sites in the TM domains of the alpha4beta2 nAChR. *Biochim Biophys Acta* **1828**(2):398-404.

Bouzat C, Bartos M, Corradi J and Sine SM (2008) The interface between extracellular and transmembrane domains of homomeric Cys-loop receptors governs open-channel lifetime and rate of desensitization. *J Neurosci* **28**(31):7808-7819.

Bradley J, Luo R, Otis TS and DiGregorio DA (2009) Submillisecond optical reporting of membrane potential in situ using a neuronal tracer dye. *J Neurosci* **29**(29):9197-9209.

Chanda B, Blunck R, Faria LC, Schweizer FE, Mody I and Bezanilla F (2005) A hybrid approach to measuring electrical activity in genetically specified neurons. *Nat Neurosci* **8**(11):1619-1626.

Chang Y, Covey DF and Weiss DS (2000) Correlation of the apparent affinities and efficacies of gamma-aminobutyric acid(C) receptor agonists. *Mol Pharmacol* **58**(6):1375-1380.

Chang Y and Weiss DS (1999) Channel opening locks agonist onto the GABAC receptor. *Nat Neurosci* **2**(3):219-225.

Chen H, Lyne PD, Giordanetto F, Lovell T and Li J (2006) On evaluating molecular-docking methods for pose prediction and enrichment factors. *J Chem Inf Model* **46**(1):401-415.

Chiara DC, Hamouda AK, Ziebell MR, Mejia LA, Garcia G, 3rd and Cohen JB (2009) [(3)H]chlorpromazine photolabeling of the torpedo nicotinic acetylcholine receptor identifies two state-dependent binding sites in the ion channel. *Biochemistry* **48**(42):10066-10077.

Chisari M, Wu K, Zorumski CF and Mennerick S (2011) Hydrophobic anions potently and uncompetitively antagonize GABA(A) receptor function in the absence of a conventional binding site. *Br J Pharmacol* **164**(2b):667-680.

Colquhoun D (1998) Binding, gating, affinity and efficacy: the interpretation of structure-activity relationships for agonists and of the effects of mutating receptors. *Br J Pharmacol* **125**(5):924-947.

daCosta CJ, Medaglia SA, Lavigne N, Wang S, Carswell CL and Baenziger JE (2009) Anionic lipids allosterically modulate multiple nicotinic acetylcholine receptor conformational equilibria. *J Biol Chem* **284**(49):33841-33849.

Demuro A, Martinez-Torres A, Francesconi W and Miledi R (1999) Antagonistic action of pitrazepin on human and rat GABA(A) receptors. *Br J Pharmacol* **127**(1):57-64.

Dey R and Chen L (2011) In search of allosteric modulators of a7-nAChR by solvent density guided virtual screening. *J Biomol Struct Dyn* **28**(5):695-715.

Estrada-Mondragon A and Lynch JW (2015) Functional characterization of ivermectin binding sites in alpha1beta2gamma2L GABA(A) receptors. *Front Mol Neurosci* **8**:55.

Estrada-Mondragon A, Reyes-Ruiz JM, Martinez-Torres A and Miledi R (2010) Structure-function study of the fourth transmembrane segment of the GABArho1 receptor. *Proc Natl Acad Sci U S A* **107**(41):17780-17784.

Fernandez Nievas GA, Barrantes FJ and Antollini SS (2008) Modulation of nicotinic acetylcholine receptor conformational state by free fatty acids and steroids. *J Biol Chem* **283**(31):21478-21486.

Hu XQ and Peoples RW (2008) Arginine 246 of the pretransmembrane domain 1 region alters 2,2,2-trichloroethanol action in the 5-hydroxytryptamine3A receptor. *J Pharmacol Exp Ther* **324**(3):1011-1018.

Hu XQ, Zhang L, Stewart RR and Weight FF (2003) Arginine 222 in the pre-transmembrane domain 1 of 5-HT3A receptors links agonist binding to channel gating. *J Biol Chem* **278**(47):46583-46589.

Kleijn WB, Bruner LJ, Midland MM and Wisniewski J (1983) Hydrophobic ion probe studies of membrane dipole potentials. *Biochim Biophys Acta* **727**(2):357-366.

Lee WY, Free CR and Sine SM (2009) Binding to gating transduction in nicotinic receptors: Cys-loop energetically couples to pre-M1 and M2-M3 regions. *J Neurosci* **29**(10):3189-3199.

Limon A, Reyes-Ruiz JM, Vaswani RG, Chamberlin AR and Miledi R (2010) Kaitocephalin antagonism of glutamate receptors expressed in Xenopus oocytes. *ACS Chem Neurosci* **1**(3):175-181.

Linsenbardt AJ, Chisari M, Yu A, Shu HJ, Zorumski CF and Mennerick S (2012) Noncompetitive, voltage-dependent NMDA receptor antagonism by hydrophobic anions. *Mol Pharmacol* **83**(2):354-366.

Martinez-Delgado G, Estrada-Mondragon A, Miledi R and Martinez-Torres A (2010) An Update on GABArho Receptors. *Curr Neuropharmacol* **8**(4):422-433.

Martinez-Torres A, Vazquez AE, Panicker MM and Miledi R (1998) Cloning and functional expression of alternative spliced variants of the rho1 gamma-aminobutyrate receptor. *Proc Natl Acad Sci U S A* **95**(7):4019-4022.

Mennerick S, Lamberta M, Shu HJ, Hogins J, Wang C, Covey DF, Eisenman LN and Zorumski CF (2008) Effects on membrane capacitance of steroids with antagonist properties at GABAA receptors. *Biophys J* **95**(1):176-185.

Miledi R (1982) A calcium-dependent transient outward current in Xenopus laevis oocytes. *Proc R Soc Lond B Biol Sci* **215**(1201):491-497.

Miledi R, Palma E and Eusebi F (2006) Microtransplantation of neurotransmitter receptors from cells to Xenopus oocyte membranes: new procedure for ion channel studies. *Methods Mol Biol* **322**:347-355.

Miller PS and Aricescu AR (2014) Crystal structure of a human GABAA receptor. *Nature* **512**(7514):270-275.

Nury H, Van Renterghem C, Weng Y, Tran A, Baaden M, Dufresne V, Changeux JP, Sonner JM, Delarue M and Corringer PJ (2011) X-ray structures of general anaesthetics bound to a pentameric ligand-gated ion channel. *Nature* **469**(7330):428-431.

Oberhauser AF and Fernandez JM (1995) Hydrophobic ions amplify the capacitive currents used to measure exocytotic fusion. *Biophys J* **69**(2):451-459.

Ochoa-de la Paz LD, Estrada-Mondragon A, Limon A, Miledi R and Martinez-Torres A (2012) Dopamine and serotonin modulate human GABArho1 receptors expressed in Xenopus laevis oocytes. *ACS Chem Neurosci* **3**(2):96-104.

Prevost MS, Sauguet L, Nury H, Van Renterghem C, Huon C, Poitevin F, Baaden M, Delarue M and Corringer PJ (2012) A locally closed conformation of a bacterial pentameric proton-gated ion channel. *Nat Struct Mol Biol* **19**(6):642-649.

Qian H, Pan Y, Zhu Y and Khalili P (2005) Picrotoxin accelerates relaxation of GABAC receptors. *Mol Pharmacol* **67**(2):470-479.

Reeves DC, Jansen M, Bali M, Lemster T and Akabas MH (2005) A role for the beta 1-beta 2 loop in the gating of 5-HT3 receptors. *J Neurosci* **25**(41):9358-9366.

Reyes-Ruiz JM, Ochoa-de la Paz LD, Martinez-Torres A and Miledi R (2010) Functional impact of serial deletions at the C-terminus of the human GABArho1 receptor. *Biochim Biophys Acta* **1798**(5):1002-1007.

Sali A and Blundell TL (1993) Comparative protein modelling by satisfaction of spatial restraints. *J Mol Biol* **234**(3):779-815.

Scott KA, Alonso DO, Sato S, Fersht AR and Daggett V (2007) Conformational entropy of alanine versus glycine in protein denatured states. *Proc Natl Acad Sci U S A* **104**(8):2661-2666.

Totrov M and Abagyan R (1997) Flexible protein-ligand docking by global energy optimization in internal coordinates. *Proteins* **Suppl 1**:215-220.

Unwin N and Fujiyoshi Y (2012) Gating movement of acetylcholine receptor caught by plunge-freezing. *J Mol Biol* **422**(5):617-634.

Velisetty P and Chakrapani S (2012) Desensitization mechanism in prokaryotic ligand-gated ion channel. *J Biol Chem* **287**(22):18467-18477.

Wang CC and Bruner LJ (1978) Lipid-dependent and phloretin-induced modifications of dipicrylamine adsorption by bilayer membranes. *Nature* **272**(5650):268-270.

Footnotes

a) This work was supported by King Abdul Aziz City for Science and Technology, Saudi Arabia [grant KACST-46749] and The University of California Institute for Mexico and United States (UC-MEXUS) [grant CN-13-613].

b) Part of this work was presented at the Society for Neuroscience 2013 meeting.

c) Agenor Limon. alimonru@uci.edu; 2226 Gillespie Neuroscience Research Facility, Irvine CA 92697.

Legends for Figures

Figure 1. Concentration dependent antagonism of DPA on GABA$_A$Rs. A. Effect of 1 mM GABA plus 100 nM DPA coapplication on GABA$_A$Rs expressed by mRNA-injected oocytes. B. Concentration-dependent antagonism of GABAρ1 receptors by DPA. C, Inhibition curves of DPA on GABA$_A$Rs (1 mM GABA) and GABAρ1 (100 µM GABA). No DPA preincubation was used for the experiments shown in A-C. IC$_{50}$ was 1.57 ± 0.2 µM for GABAρ1 (n = 4 oocytes) and 62 ± 11 nM for GABA$_A$Rs (n = 3-5 oocytes per concentration).

Figure 2. Non-competitive antagonism of DPA. A. Ion currents elicited by sequential increments of GABA concentration in absence and presence of 3 µM DPA. B. Concentration and maximal GABA currents relationship in absence and presence of 3 µM DPA. Notice that 5 µM DPA (black triangle), without preincubation, did not further reduce the fast peak of the GABA current. This indicates that without DPA preincubation the onset of DPA antagonism is always slower than the activation of GABA current. In contrast, three minutes preincubation with 3 µM DPA produced (white circles) produced a stronger, unsurmountable antagonism of GABAρ1, and three minutes preincubation with 5 µM (preDPA) reduced almost completely the maximum GABA current (white triangle at lowest right corner in the graph). Each data point is the mean ± S.E.M. of 3-6 oocytes. To avoid cumulative DPA effects only one application per oocyte was used.

Figure 3. Slow onset of DPA antagonism of GABAρ1. A. Representative GABAρ1 currents showing the effect of the DPA preincubation time on the activation of the current. B. Plot of the mean ± S.E.M. of 6 single tested oocytes per point. C, D. DPA antagonism offset in presence of GABA can be described by a single exponential function with a time constant τ of 36.2 ± 5.3 s.

29

BSA, a known scavenger of DPA, accelerated the τ of antagonism offset to 16.8 ± 1.7 s ($p = 0.014$; n = 4 oocytes) and facilitated the complete recovery of DPA antagonism upon repeated DPA applications.

Figure 4. Voltage dependence of DPA antagonism. A. DPA-induced charge movements were obtained in non-injected oocytes by applying voltage pulses from a holding potential of -90 mV to voltages between -120 to +60 mV in 10 mV steps. Traces shown in the insert were obtained by subtracting the capacitive currents in control conditions from those in presence of DPA after 3 minutes incubation. Normalized voltage dependence of DPA charge is best described by a Boltzmann equation of the form $1/[1 + \exp(V_{1/2} - V)/S]$, where $V_{1/2}$ is the half voltage for maximum charge, V is the test potential and S is the slope factor. In our experiments DPA's $V_{1/2}$ was -55 ± 2.3 mV with an S of 32.8 ± 2.5 (n = 6). B. Representative currents elicited by the ramp protocol shown in the insert. Steady-state 1 mM GABA current was obtained by subtracting the current elicited by the ramp protocol in control conditions from the ramp-elicited current after the response to 1 μM GABA reached the equilibrium. The GABA-current not blocked by 3 μM DPA was determined by subtracting ramp-elicited currents before and after 200 s incubation with DPA. C. Voltage dependence of mean fractional steady state GABA currents (dark line) available after 200 ms of DPA $\pm$ S.E.M (gray area; n = 5). Asymptotic values around the inversion potential of GABA current were omitted from the plot. D. Percentage of block at two values of voltage. E. GABA currents elicited by 1 μM GABA on oocytes clamped at negative and positive voltages. F-G. Plot of the time constants of the antagonist effect of DPA at different voltages. *** $p < 0.001$, * $p < 0.05$.

Figure 5. Differential effects of DPA on Cys-loop LGIC. Five μM DPA was preincubated for 180 s to allow adequate membrane partition. Homomeric GABAρ1, nAChα7 and 5-HT$_{3A}$

receptors were activated by 100 µM GABA, 100 µM ACh and 10 µM 5-HT, respectively. Notice that 5-HT$_{3A}$ receptors were not affected by high concentrations of DPA.

Figure 6. Docking of DPA on Cys-loop homomeric receptors. Left, Structural model of GABAρ1 interacting with DPA, the hydrophobic interaction with DPA hinders the appropriate communication of the transmembrane domains with the extracellular compartments disturbing the conformational change in the gating. Center, nAChRα7, the additional non-covalent contacts between DPA and the Cys-loop domain potentiate the activation of the channel. Right, 5-HT$_{3A}$, the loose hydrophobic interactions do not modify significantly the function of the channel.

Figure 7. Mutational analysis of GABAρ1 and DPA antagonism. Sequential reduction of the M4 and substitution of the W475 residue produced GABA receptors with distinct kinetic properties (see Table 1 for details). To evaluate DPA antagonism on the mutants, 1 µM DPA was pre-incubated for 180 s and then an EC$_{50}$ concentration of GABA was co-applied DPA. Notice the changes in the post-DPA relaxation. The removal of -3aa in the C-termini of the M4 modestly enhanced the antagonistic effect of DPA. In contrast the substitution of W475A, a substitution of an amino acid with different hydrophobicity, reduced DPA effects. C. Percentage of inhibition by DPA of the GABA-currents elicited by the different mutants studied. E. Full dose response for W475A, W475F and WT shows a larger IC$_{50}$ for W475A.

Figure 8. Analysis of correlation between the pharmacological and kinetic measures of W475 mutants. A, Time constant of current decay is faster in the mutants which also show reduced apparent affinity for GABA. B. The tail relaxation observed at the end of DPA perfusion follows a single exponential relationship with the affinity for GABA of the receptors. C. The mutants show a reduction of cooperativity, with changes in the Hill coefficient to near 1 in most of the

31

cases. The percentage of DPA inhibition did not show a clear relationship with the EC_{50}. All data

are Mean ± SEM. The lines in A and B are the linear and exponential fit to the experimental

data. The coefficient of correlation for each curve is shown as insert.

Table 1. Properties of GABAρ1 mutants

Receptor	N	EC_{50} (µM) for GABA	Hill	N	GABA current at the [EC_{50}] (nA)	Tau of current activation (s)	Tau of current decay (s)
WT	5	0.73 ± 0.14	3.0 ± 0.5	6	3945 ± 206	5.1 ± 2.8	22.1 ± 0.8
-1aa	3	0.41 ± 0.05	3.0 ± 0.1	6	2279 ± 479***	11.6 ± 0.8***	28.2 ± 0.9***
-2aa	3	2.16 ± 0.06**	3.9 ± 0.7	6	5246 ± 109***	2.4 ± 0.1**	6.2 ± 0.1 ***
-3aa	3	1.26 ± 0.15	1.4 ± 0.1**	6	604 ± 129***	7.1 ± 0.1*	22.8 ± 0.7
W475F	12	4.08 ± 0.49***	1.6 ± 0.1**	5	879 ± 91***	3.6 ± 0.2	6.3 ± 0.4***
W475L	4	1.72 ± 0.24**	2.3 ± 0.02	5	620 ± 65***	4.5 ± 0.5	12.4 ± 0.4***
W475A	4	2.72 ± 0.35***	1.4 ± 0.2**	6	634 ± 57***	4.6 ± 1.0	11.0 ± 1.1***
W475G	4	3.30 ± 0.12 ***	1.4 ± 0.1**	5	54 ± 7***	3.5 ± 0.2	11.7 ± 1.1***
W465R	3	NR	NR	3	ND	NR	NR
W475D	3	NR	NR	3	ND	NR	NR

NR, no response to GABA; ND, no determined. Rise time is the tau activation mean ± S.E.M., of the EC_{50} current. Statistical comparison using Dunnett's method.* $p < 0.05$, ** $p < 0.005$, *** $p < 0.0001$.
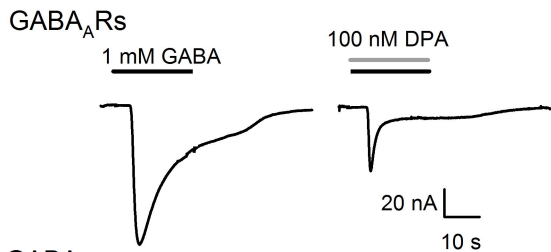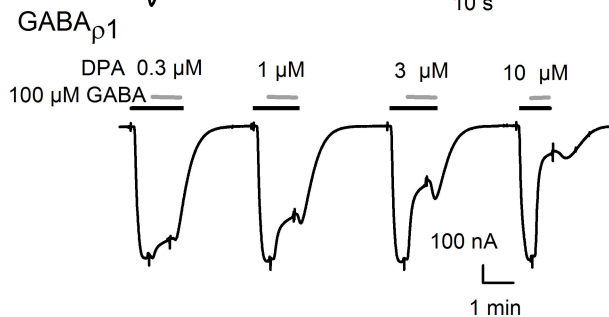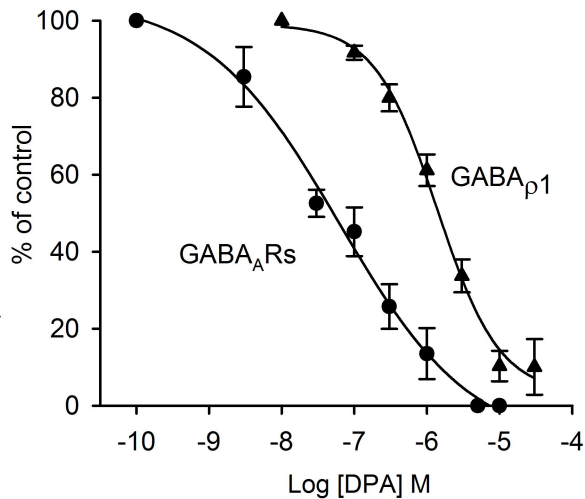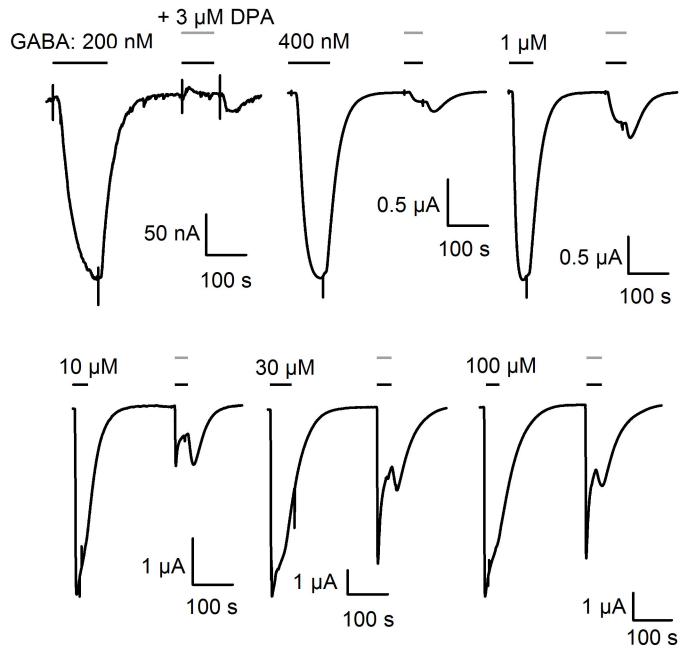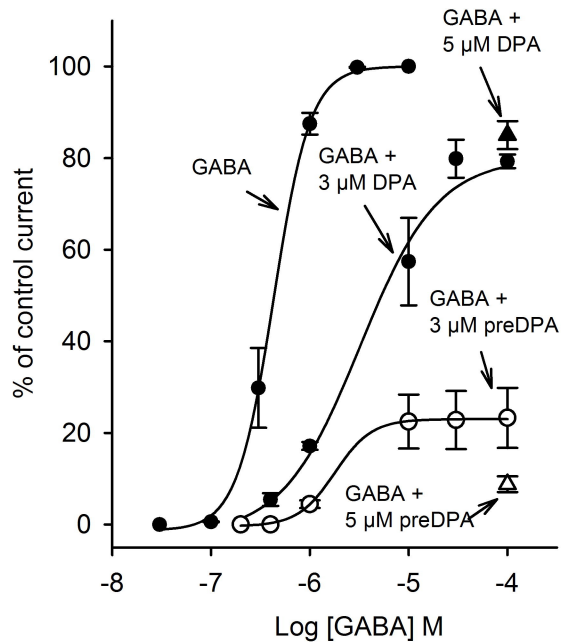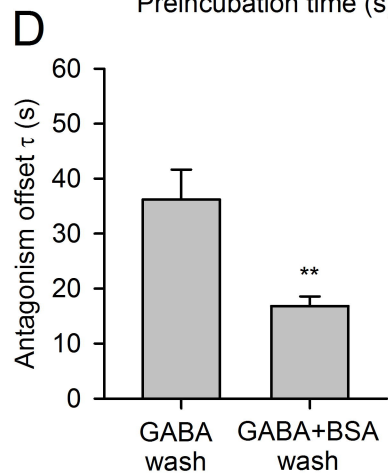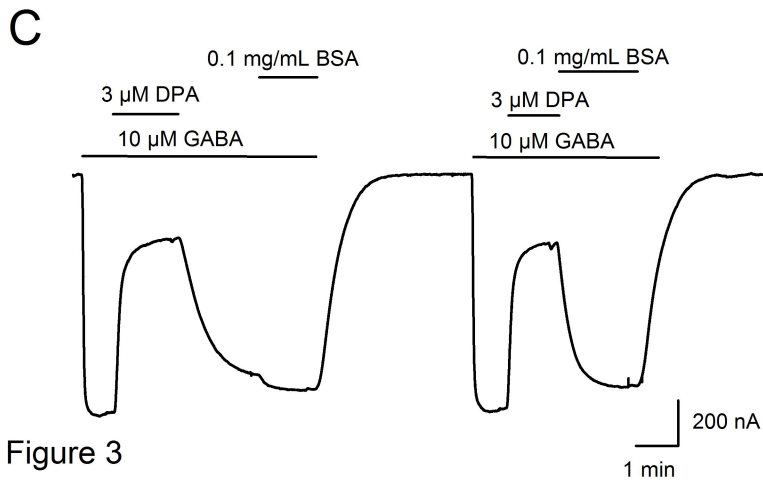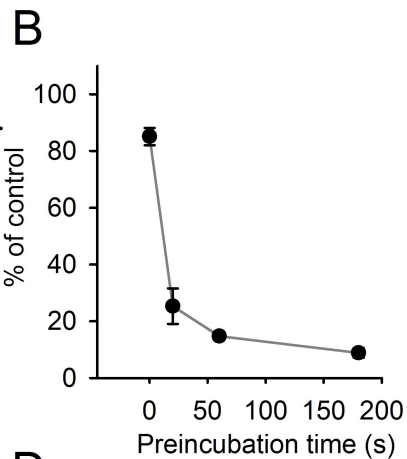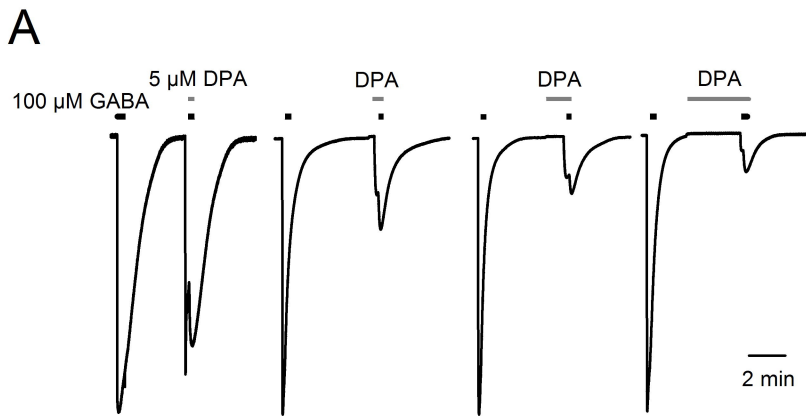
Figure 1

Figure 2

Figure 3

Figure 4

Figure 5

GABA ρ1   nACh α7   5-HT3

GABA ρ1 panel labels: I281, L207, L285, F478, Y289, W475, DPA, Y474

nACh α7 panel labels: R227, F157, DPA, F493, F159, Y296, F297

5-HT3 panel labels: F166, F164, DPA1, DPA2, W472, F309

Figure 6

Figure 7

Figure 8